Supplementary material

Experimental

$(ZnO)_{1-x}(GaN)_x$ thin films were deposited on (0001) a-Al_2O_3 substrates, using a Moorfield Minilab magnetron sputtering system with separate ZnO (99.999% purity) and GaN (99.99% purity) 3 inch ceramic targets. Prior to deposition, the sapphire substrates were cleaned by annealing in oxygen atmosphere for 1 h at 1150 ^{o}C, before the samples were loaded into the sputter chamber. The base pressure prior to deposition was below $2x10^{-6}$ Torr before deposition was started, while the pressure during deposition was kept at 7 mTorr. The substrate temperature was kept at 400 ^{o}C and the sample stage was rotated at 11 rpm to ensure good film uniformity. In order to remove surface impurities from the targets, a pre-sputtering cleaning was carried out for 20 min before deposition. During the co-sputtering process, where the ZnO and GaN targets are running simultaneously, the composition of the film was controlled by applying different voltages to the two targets, in addition to controlling the gas flows of Ar and N_2 in the chamber. In particular, the $x = 0.15$ composition was obtained by applying 30W and 20W to the ZnO and GaN targets respectively, while gas flows of 12.5 sccm Ar and 5 sccm N_2 (required in the sputtering chamber for a stoichiometric composition) were kept constant during deposition. Furthermore, a reduced N_2 gas flow at 2.5 sccm -while keeping the other deposition parameters the same- was applied in order to investigate its influence on the film properties. Post-deposition isochronal anneals were performed for one hour in nitrogen atmosphere at 600, 700, and 800 ^{o}C.

STEM, EELS and EDX investigations were conducted on an FEI Titan G2 60-300 kV equipped with a CEOS DCOR probe-corrector, monochromator and Super-X EDX detectors. Observations were performed at 300 kV with a probe convergence angle of 24 mrad. The camera length was set to 77 mm and simultaneous STEM imaging was conducted with 3 detectors: HAADF (collection angles 98.7-200 mrad), ADF (collection angles 21.5-98.7 mrad) and ABF (collection angles 10.6-21.5 mrad). The resulting spatial resolution achieved was approximately 0.08 nm. EELS was performed using a Gatan Quantum 965 imaging filter. The energy dispersion was 0.1 eV/channel and the energy resolution measured using the full width at half maximum (FWHM) of the zero-loss peak was 1.1 eV. Electron transparent TEM samples with a cross-sectional wedge geometry were prepared by mechanical grinding and polishing (Allied MultiPrep). Final thinning was performed by Ar ion milling with a Fishione Model 1010, and plasma cleaning was applied directly before the TEM investigations, with a Fishione Model 1020. The sample thickness (t) was evaluated by low-loss EELS according to $\frac{t}{\lambda} = ln(\frac{I_t}{I_0})$, where λ is the inelastic mean free path, I_t the intensity of the entire spectrum and I_0 the intensity of the zero loss peak. The sample thickness was estimated to be ~10 nm using this method.

Results

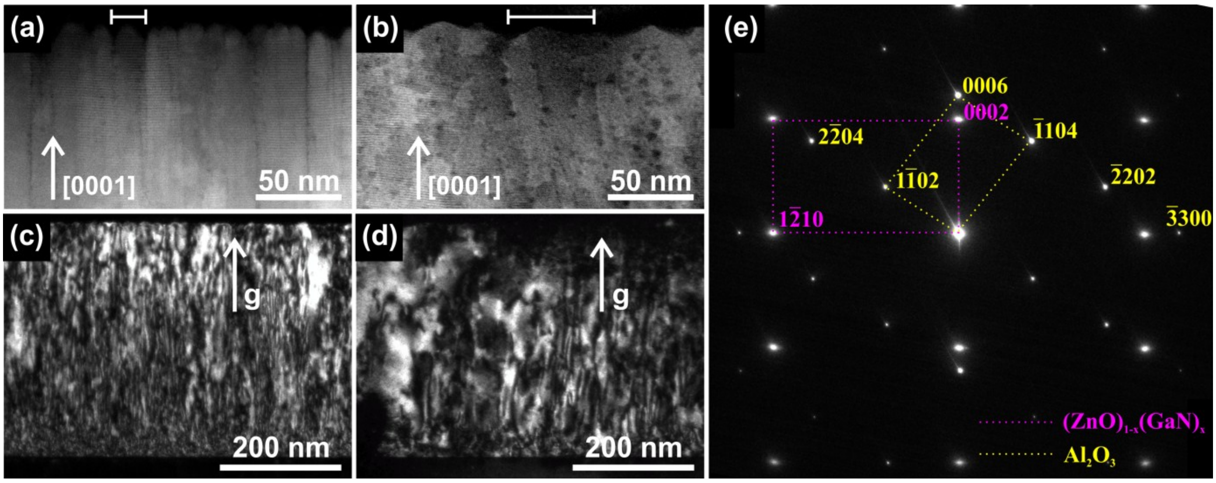

S1: (a)-(b) ADF-STEM images recorded close to the surface of the $(ZnO)_{0.85}(GaN)_{0.15}$ thin films before and after thermal annealing respectively. (c)-(d) TEM WBDF g/3g images obtained under two-beam conditions with g0002 before and after thermal annealing respectively. A clear increase in the grain size is observed after annealing, resulting in an improved crystal quality of the films, with lower threading dislocation (TD) density. (e) Selected Area Electron Diffraction (SAED) pattern revealing a highly crystalline single-domain film of wurtzite phase, exhibiting a good heteroepitaxial relationship with the (0001) a-Al_2O_3 substrate described by: $[0001]_{(ZnO)0.85(GaN)0.15}//[0001]_{Al2O3}$ (out-of-plane) and $[10\text{-}10]_{(ZnO)0.85(GaN)0.15}//[11\text{-}20]_{Al2O3}$ (in-plane). This relationship implies a 30° in-plane rotation of the film unit cell with respect to that of the substrate (the so-called 'aligned domain'). This orientation relationship is favourable since it results in a reduction of mismatch ($(d_f–d_s)/d_s$, where d_f and d_s denote the interplanar spacing of the film and substrate, respectively) from 32% to 18%.

Regarding the comparison of TD density, careful characterization was performed, working in TEM-mode under two-beam conditions using the **weak-beam dark field g/3g method** (WBDF). This method is ideal for characterization of extended defects, due to a small excitation error, so defects as TDs are better resolved. According to the invisibility criterion *g.b* (where b is the Burgers vector), we can identify the TD-type working under different two-beam conditions. The comparison was made in areas having the same thickness along the viewing direction.

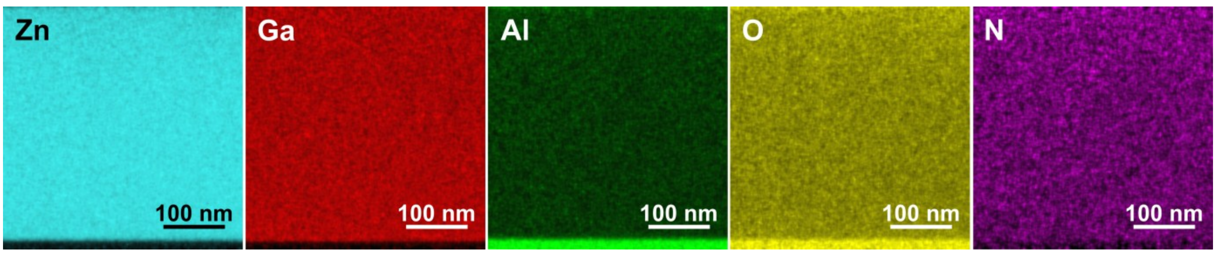

S2: EDX maps carried out in STEM-mode with 5 nm pixel size. The annealed films are random alloys on the meso-scale, exhibiting a homogeneous elemental distribution with no indication of phase separation phenomena and intense elemental clustering.

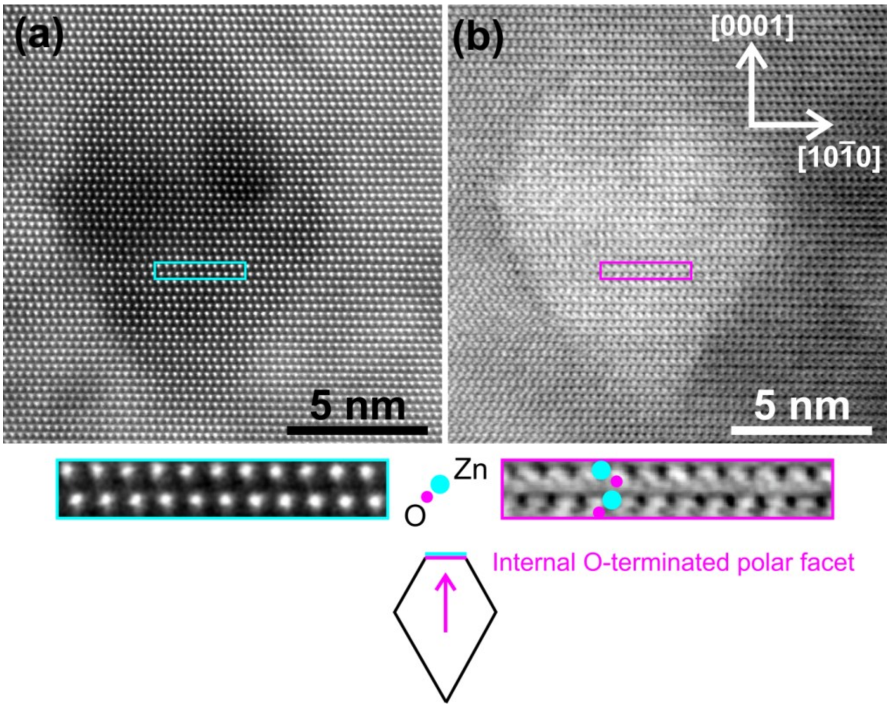

S3: (a) HAADF-STEM and (b) ABF-STEM images of a void recorded simultaneously. In HAADF only atomic columns of heavy elements (Zn and Ga) are detected while ABF provides visualization of both heavy and light elements (Zn, Ga, O, N). By resolving the Zn-O dumbbells the polarity is identified as Zn-faced ([0001] growth direction). Hence the polar facets that are stabilized at the voids are the O-terminated internal facets along with the semi-polar ones.

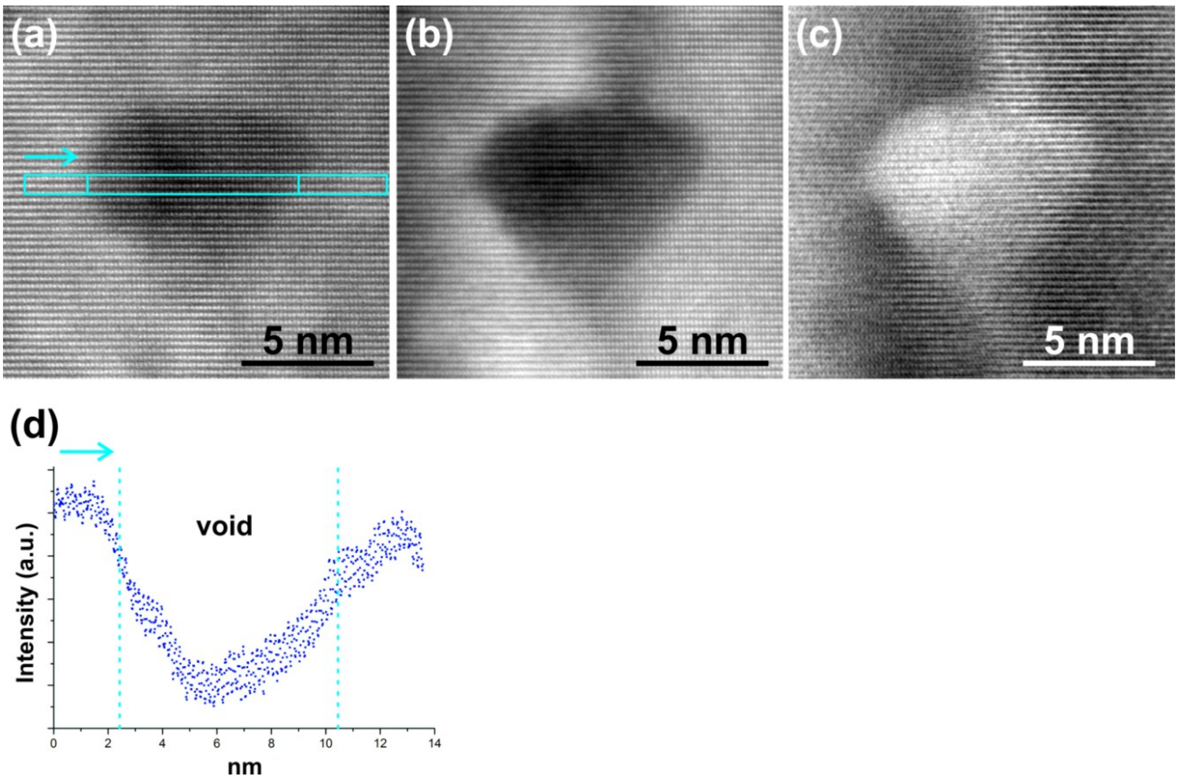

S4: (a) HAADF-STEM, (b) ADF-STEM and (c) ABF-STEM images of a void recorded simultaneously. (d) the intensity profile in HAADF indicates a clear drop in the Z-contrast crossing the void.

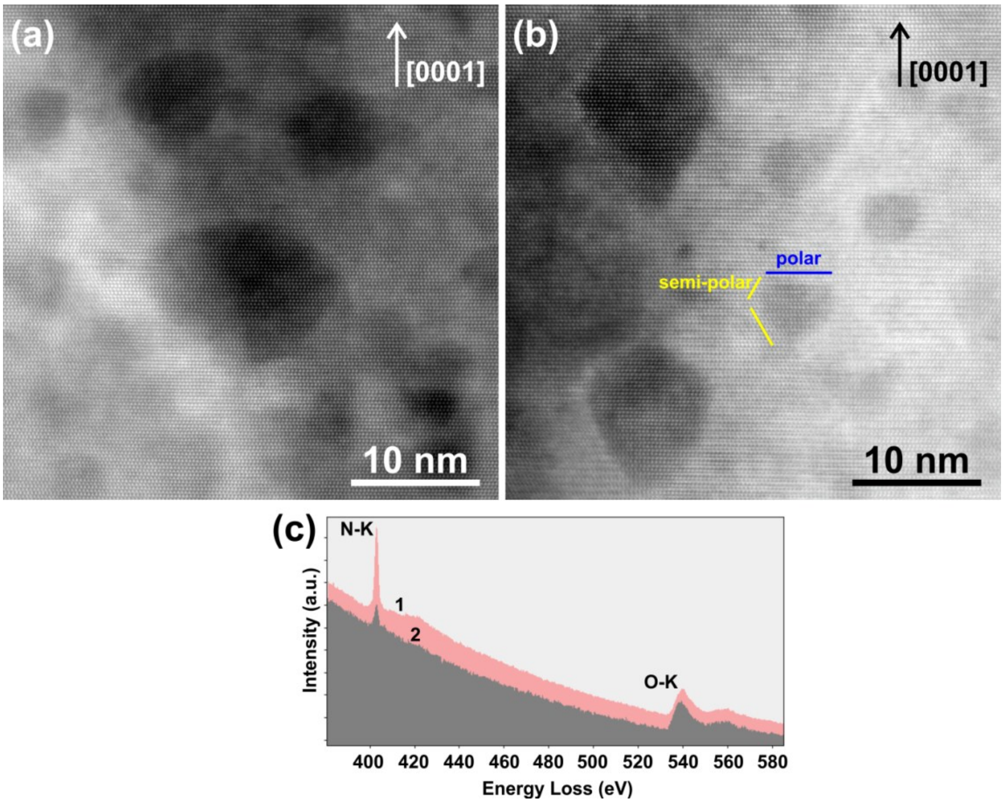

S5: ADF-STEM images showing voids in the case of (a) 5 sccm N_2 flow and (b) 2.5 sccm N_2 flow. In case (a), the voids were filled with N_2 and the facets exhibited more round shape. In case (b), weak (or zero) N-K signals were detected and the voids exhibited well-defined facets even at smaller sizes. It is evident that the facets on the polar {0001} planes appear only in the small voids, while the energetically favorable facets on semi-polar planes prevail as the voids grow in size. (c) Comparison of two EELS spectra (1) from a round void as shown in (a) and (2) from a sharply-faceted void as shown in (b).